Article:
Yanes, R., Chubykalo-Fesenko, O., Kachkachi, H. et al. (4 more authors) (2007) Effective anisotropies and energy barriers of magnetic nanoparticles with Néel surface anisotropy. Physical Review B. 064416. ISSN 2469-9969

https://doi.org/10.1103/PhysRevB.76.064416

Effective anisotropies and energy barriers of magnetic nanoparticles with Néel's surface anisotropy

R. Yanes and O. Chubykalo-Fesenko
Instituto de Ciencia de Materiales de Madrid, CSIC, Cantoblanco, 28049 Madrid, Spain

H. Kachkachi
Groupe d'Etude de la Matière Condensée, Université de Versailles St. Quentin, CNRS UMR8634, 45 av. des Etats-Unis, 78035 Versailles, France

D. A. Garanin
Department of Physics and Astronomy, Lehman College, City University of New York, 250 Bedford Park Boulevard West, Bronx, New York 10468-1589, U.S.A.

R. Evans and R. W. Chantrell
Department of Physics, University of York, Heslington, York YO10 5DD, UK

Magnetic nanoparticles with Néel surface anisotropy, different internal structures, surface arrangements and elongation are modelled as many-spin systems. The results suggest that the energy of many-spin nanoparticles cut from cubic lattices can be represented by an effective one-spin potential containing uniaxial and cubic anisotropies. It is shown that the values and signs of the corresponding constants depend strongly on the particle's surface arrangement, internal structure and elongation. Particles cut from a simple cubic lattice have the opposite sign of the effective cubic term, as compared to particles cut from the face-centered cubic lattice. Furthermore, other remarkable phenomena are observed in nanoparticles with relatively strong surface effects: (i) In elongated particles surface effects can change the sign of the uniaxial anisotropy. (ii) The competition between the core and surface anisotropies leads to a new energy that contributes to both the $2^{\rm nd}-$ and $4^{\rm th}-$order effective anisotropies.

We also evaluate energy barriers ΔE as functions of the strength of the surface anisotropy and the particle size. The results are analyzed with the help of the effective one-spin potential, which allows us to assess the consistency of the widely used formula $\Delta E/V = \mathcal{K}_\infty + 6\mathcal{K}_s/D$, where $\mathcal{K}_\infty$ is the core anisotropy constant, $\mathcal{K}_s$ is a phenomenological constant related to surface anisotropy, and D is the particle's diameter. We show that the energy barriers are consistent with this formula only for elongated particles for which the surface contribution to the effective uniaxial anisotropy scales with the surface and is linear in the constant of the Néel surface anisotropy.

PACS numbers: 75.75.+a, 75.10.HK

I. INTRODUCTION

Understanding the thermally-activated switching of magnetic nanoparticles is crucial to many technological applications and is challenging from the point of view of basic research. Surface effects have a strong bearing on the behavior of magnetic nanoparticles. They exist almost inevitably due to many physical and chemical effects including crystallographic arrangement on the surface, oxidation, broken surface bonds, existence of surfactants, etc. Magnetic particles are often embedded in non-magnetic matrices which alter magnetic properties of the surface in many ways such as additional surface tension and possible charge transfer.

Consequently, the properties of magnetic particles are not the same as those of the bulk material, and many experiments have shown an increase in the effective magnetic anisotropy due to surface effects[1–4]. Quantum *ab-initio* studies have revealed different anisotropy and magnetic moment at the surface of magnetic clusters embedded in matrices[5]. Synchrotron radiation studies have confirmed that both spin and orbital moments at the surface differ significantly from their bulk counterparts[6]. Recent μ-SQUID experiments on isolated clusters[1,2] produced more reliable estimations of surface anisotropy.

Thermal measurements have become an important part of the characterization of systems of magnetic nanoparticles. Often, these measurements include a complex influence of inter-particle interactions. However, in other cases, measurements on dilute systems can provide information on individual particles. The results show that even in these cases the extracted information is not always consistent with the approximation picturing the particle as a macroscopic magnetic moment, and this is usually attributed to surface effects.

Experimentally, the enhancement of the anisotropy at the surface often leads to an increase in the blocking temperature of single-domain particles from which the values of the energy barriers ΔE may be extracted. The influence of the surface manifests itself in the fact that the

values $\Delta E/V$ are different from that of the bulk, i.e., there is an effective anisotropy $\mathcal{K}_{\rm eff}$ that is not exactly proportional to the particle's volume V.

One can expect that the effect of the surface reduces when the particle size increases. In Ref. 3 it was suggested that the effective anisotropy scales as the inverse of the particle's diameter D according to

$$\Delta E/V = \mathcal{K}_{\rm eff} = \mathcal{K}_\infty + \frac{6\mathcal{K}_s}{D}. \tag{1}$$

anisotropy, and $\mathcal{K}_s$ is the "effective" surface anisotropy. We would like to emphasize that this formula has been introduced in an *ad hoc* manner, and it is far from evident that the surface should contribute into an effective uniaxial anisotropy (related to the barrier ΔE) in a simple additive manner. Actually one cannot expect $\mathcal{K}_s$ to coincide with the atomistic single-site anisotropy, especially when strong deviations from non-collinearities leading to 'hedgehog-like' structures appear[7]. The effective anisotropy $\mathcal{K}_{\rm eff}$ appears in the literature in relation to the measurements of energy barriers, extracted from the magnetic viscosity or dynamic susceptibility measurements. The surface anisotropy should affect both the minima and the saddle point of the energy landscape in this case. The origin of $\mathcal{K}_{\rm eff}$ may be expected to be different from that obtained from, e. g., magnetic resonance measurements. In the latter case the magnetization dynamics depends on the stiffness of the energy minima modified by the surface effects. Despite its *ad hoc* character, Eq. (1) has become the basis of many experimental studies with the aim to extract the surface anisotropy from thermal magnetization measurements (see, e.g., Refs. 4,10,11) because of its mere simplicity. Up to now there were no attempts to assess the validity of Eq. (1) starting from an atomistic surface anisotropy models such as the Néel surface anisotropy.

The aim of the present paper is to understand the influence of the Néel surface anisotropy on the behavior of magnetic particles with different surface arrangements, shapes and sizes. Although various crystal structures have been investigated, the overall particle properties were kept close to Co. With the help of numerical modelling of magnetic particles as many-spin systems, we show that the energy of the many-spin particle can be effectively represented by that of an effective one-spin particle with both uniaxial and cubic anisotropy terms. The effective anisotropy constants depend on the surface arrangement of the particle, crystal structure, and elongation. We numerically evaluate the energy barriers of many-spin particles and show that they can also be understood in terms of the effective one-spin approximation. Incidentally, this allows us to establish the conditions for the validity of Eq. (1) which turns out to correctly describe the magnetic behavior of elongated particles only.

II. FROM THE ATOMISTIC TO THE EFFECTIVE ENERGY

A. The atomistic model

We consider the atomistic model of a magnetic nanoparticle consisting of $\mathcal{N}$ classical spins $\mathbf{s}_i$ (with $|\mathbf{s}_i| = 1$) taking account of its lattice structure, shape, and size[7,12,14–21]. The magnetic properties of the particle can be described by the anisotropic Heisenberg model

$$\mathcal{H} = -\frac{1}{2} J \sum_{ij} \mathbf{s}_i \cdot \mathbf{s}_j + \mathcal{H}_{\rm anis}, \tag{2}$$

where J is the nearest-neighbor exchange interaction and $\mathcal{H}_{\rm anis}$ contains core and surface anisotropies.

The surface anisotropy is often thought to favor the spin orientation normal to the surface. This is the so-called transverse anisotropy model (TSA). However, a more solid basis for understanding surface effects is provided by the Néel surface anisotropy (NSA),[1,8,9,18] which takes into account the symmetry of local crystal environment at the surface. The simplest expression for the NSA that will be used below is, as the exchange energy, a double lattice sum over nearest neighbors i and j,

$$\mathcal{H}_{\rm anis}^{\rm NSA} = \frac{K_s}{2} \sum_{ij} \left(\mathbf{s}_i \cdot \mathbf{u}_{ij}\right)^2, \tag{3}$$

where $\mathbf{u}_{ij}$ are unit vectors connecting neigboring sites. One can see that for perfect lattices the contributions of the bulk spins into $\mathcal{H}_{\rm anis}^{\rm NSA}$ yield an irrelevant constant, and the anisotropy arising for surface spins only because of the local symmetry breaking is, in general, biaxial. For the simple cubic (sc) lattice and the surface parallel to any of crystallographic planes, an effective transverse surface anisotropy arises for $K_s > 0$. In all other cases NSA cannot be reduced to TSA. In fact, Eq. (3) can be generalized so that it describes both surface and bulk anisotropy. It is sufficient to use different constants K_s for different bond directions $\mathbf{u}_{ij}$ to obtain a second-order volume anisotropy as well. However, to obtain a cubic volume anisotropy that is fourth order in spin components, a more serious modification of Eq. (3) is required. Thus, for simplicity, we will simply use Eq. (3) to describe the surface anisotropy and add different kinds of anisotropy in the core.

For the core spins, i.e., those spins with full coordination, the anisotropy energy $\mathcal{H}_{\rm anis}$ is taken either as uniaxial with easy axis along z and a constant K_c (per atom), that is

$$\mathcal{H}_{\rm anis}^{\rm uni} = -K_c \sum_i s_{i,z}^2, \tag{4}$$

or cubic,

$$\mathcal{H}_{\rm anis}^{\rm cub} = \frac{1}{2} K_c \sum_i \left(s_{i,x}^4 + s_{i,y}^4 + s_{i,z}^4\right). \tag{5}$$

Dipolar interactions are known to produce an additional "shape" anisotropy. However, in the atomistic description, their role in describing the spin noncollinearities is negligible as compared to that of all other contributions. In order to compare particles with the same strength of anisotropy in the core, we assume that the shape anisotropy is included in the core uniaxial anisotropy contribution. We also assume that in the ellipsoidal particles the magnetocrystalline easy axis is parallel to the elongation direction.

In magnetic nanoparticles or nanoclusters, the number of surface spins N_s is comparable to or even larger than the number of core spins N_c. In addition, the surface anisotropy has a much greater strength than the core anisotropy because of the local symmetry breaking. We use the core anisotropy value typical for Cobalt, $K_c \simeq 3.2 \times 10^{-24}$ Joule/atom. Numerous experimental results[4,10,11,13] show that the value of the surface anisotropy in Co particles embedded in different matrices such as alumina, Ag or Au, as well as in thin films and multilayers, could vary from $K_s \simeq 10^{-4}J$ to $K_s \simeq J$. In the present study we will consider the surface anisotropy constant K_s as a variable parameter. For illustration we will choose values of K_s 10-50 times larger than that of the core anisotropy, in accordance with those reported in Ref. 4 for Co particles embedded into alumina matrices. Such values of K_s are also compatible with those reported in Refs. 29–31. All physical constants will be measured with respect to the exchange coupling J, so we define the following reduced anisotropy constants

$$k_c \equiv K_c/J, \quad k_s \equiv K_s/J. \tag{6}$$

The core anisotropy constant will be taken as $k_c \simeq 0.01$ and $k_c \simeq 0.0025$. On the other hand, the surface anisotropy constant k_s will be varied. Note that we are using atomistic temperature-independent constants for anisotropies that should not be confused with temperature-dependent micromagnetic anisotropy constants $K(T)$. The relation between atomistic and micromagnetic uniaxial anisotropy constants within the mean-field approximation can be found in Ref. 32.

B. The effective energy

Investigation of the magnetization switching of a particle consisting of many atomic spins is challenging because of the multidimensionality of the underlying potential that can have a lot of minima of different topologies, connected by sophisticated paths. Examples are the 'hedgehog' structures realized in the case of a strong enough surface anisotropy that causes strong noncollinearity of the spins. Obviously in this case Eq. (1), relevant in the one-spin description of the problem, cannot be a good approximation. Thus an important question that arises here is whether it is possible to map the behavior of a many-spin particle onto that of a simpler model system such as one effective magnetic moment. Such an analysis is unavoidable since it is a crucial step in calculating relaxation rates and thereby in the study of the magnetization stability against thermally-activated reversal.

In the practically important case of dominating exchange interaction, and thus only a small noncollinearity of the spins, the problem dramatically simplifies, so that the initial many-spin problem can be reduced to an effective one-spin problem (EOSP). In the first approximation, one can consider spins as collinear and calculate the contribution of the surface anisotropy to the energy of the system depending on the orientation of its global magnetization $\mathbf{m}$, ($|\mathbf{m}| = 1$). The resulting energy scales as the number of surface spins, is linear in K_s and depends on the crystal structure and shape. This is we refer to as the first-order surface-anisotropy energy $\mathcal{E}_1$. Together with the core anisotropy energy (per spin)

$$\mathcal{E}_c = \frac{N_c}{\mathcal{N}} K_c \begin{cases} -m_z^2, & \text{uniaxial} \\ \frac{1}{2}\left(m_x^4 + m_y^4 + m_z^4\right), & \text{cubic} \end{cases} \tag{7}$$

$\mathcal{E}_1$ can lead to Eq. (1). However, for crystal shapes such as spheres or cubes $\mathcal{E}_1$ vanishes by symmetry. In Ref.[18] was shown that for an ellipsoid with axes a and $b = a(1+\epsilon)$, $\epsilon \ll 1$, cut out of a sc lattice so that the ellipsoid's axes are parallel to the crystallographic directions, the first-order anisotropy is given by

$$\mathcal{E}_1 = -K_{\rm ua} m_z^2, \qquad K_{\rm ua} \sim -\frac{N_s}{\mathcal{N}} K_s \epsilon. \tag{8}$$

That is, it scales with particle size as $\sim 1/\mathcal{N}^{1/3} \sim 1/D$. One can see that, for the uniaxial core anisotropy along the elongation direction of the ellipsoid, $K_s < 0$ and $\epsilon > 0$, Eq. (1) follows. On the contrary, in other cases, as for example, $\epsilon > 0, K_s > 0$ Eq. (1) is not obtained.

If one takes into account the noncollinearity of the spins that results from the competition of the exchange interaction and surface anisotropy and is described by the angles of order $\delta\psi \sim \mathcal{N}^{1/3} K_s/J$, a contribution of second order in K_s arises in the particle effective energy.[18] The spin noncollinearity depends on the orientation of $\mathbf{m}$ and results in the effective cubic anisotropy

$$\mathcal{E}_2 = K_{\rm ca}\left(m_x^4 + m_y^4 + m_z^4\right), \qquad K_{\rm ca} \sim \kappa \frac{K_s^2}{zJ}, \tag{9}$$

where z is the number of nearest neighbors and for the sc lattice one has $\kappa \simeq 0.53466$. This equation was obtained analytically for $K_s \ll J$ in the range of particle sizes large enough ($\mathcal{N} \gg 1$) but small enough so that $\delta\psi$ remains small. Numerical calculations yield $K_{\rm ca}$ slightly dependent on the size since the applicability conditions for Eq. (9) are usually not fully satisfied. The ratio of the second- to first-order surface contributions is

$$\frac{\mathcal{E}_2}{\mathcal{E}_1} \sim \frac{K_s}{J} \frac{\mathcal{N}^{1/3}}{\epsilon}. \tag{10}$$

It can be significant even for $K_s \ll J$ due to the combined influence of the large particle size and small deviation from symmetry, $\epsilon \ll 1$. Since $K_{\rm ca}$ is nearly size

independent (i.e., the whole energy of the particle scales with the volume), it is difficult to experimentally distinguish between the core cubic anisotropy and that due to the second-order surface contribution (see discussion later on). The reason for the size independence of $K_{\rm ca}$ is the deep penetration of spin noncollinearities into the core of the particle. This means that the angular dependence of the non collinear state also contributes to the effective anisotropy. Interestingly this implies that the influence of the surface anisotropy on the overall effective anisotropy is not an isolated surface phenomena and is dependent on the magnetic state of the particle. We note that this effect is quenched by the presence of the core anisotropy which could screen the effect at a distance of the order of domain wall width from the surface.

Taking into account the core anisotropy analytically to describe corrections to Eq. (9) due to the screening of spin noncollinearities in the general case is difficult. However, one can consider this effect perturbatively, at least to clarify the validity limits of Eq. (9). One obtains[27] an additional mixed contribution that is second order in K_s and first order in K_c

$$\mathcal{E}_{21} = K_{\rm csm}\, g(\mathbf{m}), \qquad K_{\rm csm} \sim \tilde{\kappa} N_s \frac{K_c K_s^2}{J^2} \tag{11}$$

where $g(\mathbf{m})$ is a function of m_α which comprises, among other contributions, both the $2^{\rm nd}$- and $4^{\rm th}$-order contributions in spin components[27]. For example for sc lattice, $g(\theta, \varphi = 0) = -\cos^2\theta + 3\cos^4\theta - 2\cos^6\theta$, which is shown later to give agreement with numerical simulations. This mixed contribution, called here the *core-surface mixing* (CSM) contribution, should satisfy $K_{\rm csm} \lesssim K_{\rm ca}$ which requires

$$N_s K_c / J \lesssim 1. \tag{12}$$

This is exactly the condition that the screening length (i.e., the domain-wall width) is still much greater than the linear size of the particle, $\delta \sim \sqrt{J/K_c} \gtrsim D \sim \mathcal{N}^{1/3}$. For too large sizes the perturbative treatment becomes invalid.

Thus we have seen that in most cases the effective anisotropy of a magnetic particle, considered as a single magnetic moment, can be approximately described as a combination of uniaxial and cubic anisotropies[18,21,27]. Consequently, collecting all these contributions and defining the EOSP energy as

$$\mathcal{E}_{\rm EOSP} = \frac{1}{J}(\mathcal{E}_c + \mathcal{E}_1 + \mathcal{E}_2 + \mathcal{E}_{21}) \tag{13}$$

one can model the energy of a many-spin particle as

$$\mathcal{E}_{\rm EOSP} = -k_{\rm ua}^{\rm eff} m_z^2 - \frac{1}{2} k_{\rm ca}^{\rm eff} \sum_{\alpha=x,y,z} m_\alpha^4. \tag{14}$$

The subscripts ua/ca stand for uniaxial/cubic anisotropy, respectively. The effective anisotropy constants are normalized to the exchange constant J, according to the definition Eq. (6). Note that we have changed the sign of the cubic anisotropy constant to be consistent with more customary notations. We note that due to the contributions from Eqs. (8) and (11), even if the core anisotropy is not uniaxial, the effective energy contains two uniaxial contributions induced by the surface, a large contribution that is due to elongation given by Eq. (8) and a much weaker contribution owing to the mixing between the core and the surface given by Eq. (11). Indeed, in Ref. 21, where the energy of a many-spin spherical particle with uniaxial anisotropy in the core and TSA on the surface was computed using the Lagrange-multiplier technique, it turned out that the core anisotropy is modified. We may attribute this effect to the CSM contribution.

Therefore, the $2^{\rm nd}$-order term with the coefficient $k_{\rm ua}^{\rm eff}$ in Eq. (14) stems from the two contributions (8) and (11). Similarly, the $4^{\rm th}$-order term with the coefficient $k_{\rm ca}^{\rm eff}$ comprises the contribution (9) from the surface, and part of the CSM contribution in Eq. (11), and also a contribution from the core if the latter has a cubic anisotropy.

We now are going to numerically calculate the effective energy of spherical, ellipsoidal and truncated octahedral magnetic particles cut from a lattice with sc, fcc, and hcp structures. We will plot this energy as a function of the polar angles of the net magnetic moment $\mathbf{m}$ of the particle and fit it to Eq. (14). From these fits we extract the effective anisotropy constants $k_{\rm ua}^{\rm eff}$ and $k_{\rm ca}^{\rm eff}$ and compare their behavior with those predicted by the analytical formulas discussed above in the case of the sc lattice. We will investigate the differences between the results for different lattice structures and crystal shapes.

III. NUMERICAL METHOD AND RESULTS

A. Computing method

As mentioned above, the problem of studying the multidimensional energy landscape of the multispin particle is, in general, very difficult. However, if the exchange J is dominant over the anisotropy and the spin noncollinearity is small, one can, to a good approximation, describe the particle by its net or global magnetization $\mathbf{m}$ ($|\mathbf{m}| = 1$) as a slow master variable. All other variables such as spin noncollinearities quickly adjust themselves to the instantaneous direction of $\mathbf{m}$. Thus one can treat the energy of the particle as a function of $\mathbf{m}$ only. Technically this can be done with the help of the Lagrange multiplier technique[18] by considering the augmented energy $\mathcal{F} = \mathcal{H} - \mathcal{N}\boldsymbol{\lambda}\cdot(\boldsymbol{\nu} - \mathbf{m})$, where $\boldsymbol{\nu} \equiv \sum_i \mathbf{s}_i / |\sum_i \mathbf{s}_i|$ and $\mathcal{H}$ is the atomistic energy of the particle, Eq. (2). The Lagrange-multiplier term produces an additional torque on the atomic spins that forces the microscopic net magnetization $\boldsymbol{\nu}$ to coincide with $\mathbf{m}$. The equilibrium state of the spin system is determined by solving the Landau-Lifshitz equation (without the precession term and with the damping coefficient $\alpha = 1$) and an additional equa-

tion for λ

$$\frac{d\mathbf{s}_i}{dt} = -\left[\mathbf{s}_i \times [\mathbf{s}_i \times \mathbf{F}_i]\right], \qquad \frac{d\lambda}{dt} = -\mathcal{N}(\nu - \mathbf{m}), \quad (15)$$

where the effective field $\mathbf{F}_i = -\partial\mathcal{F}/\partial\mathbf{s}_i$ depends on λ. It is worth noting that the stationary points of $\mathcal{F}$ found with this method are also stationary points of the actual Hamiltonian $\mathcal{H}$. Indeed, for these orientations of $\mathbf{m}$ no additional torque is needed to support this state, thus the solution of our equations yields $[\lambda \times \mathbf{m}] = 0$. For all other directions, the unphysical Lagrange-multiplier field introduces distortions of the microscopic spin configuration. Nevertheless, if the exchange is dominant, these distortions remain small. A further advantage of this technique is that it can produce highly non-collinear multidimensional stationary points[18,21,22] in the case of strong surface anisotropy. Here, again, these stationary points are true points because of the condition $[\lambda \times \mathbf{m}] = 0$. In order to check the correct loci of the saddle points, we computed the eigenvalues and gradients of the Hessian matrix associated with the Hamiltonian of Eq. (2), with the results that are exactly the same as those obtained by the much simpler Lagrange-multiplier method. We stress that previous researchers (see, e.g., Ref. 2), ignore the effect of spin non-collinearities.

In this work we show that the magnetic behavior of small particles is very sensitive to the surface arrangement, shape of the particles and underlying crystallographic structure. To investigate the various tendencies, we have considered particles cut from lattices with the simple cubic (sc), body-centered cubic (bcc), face-centered cubic (fcc), hexagon closed-packed (hcp). Although experimental studies providing transmission electron microscopy images show particles resembling truncated octahedra[1,2], making realistic particle shapes and surface arrangements proves to be rather complex. Truncated octahedra have been included in our studies as an ideal case for fcc crystals. The reality is somewhat more complicated, though. In Ref. 2, in order to interpret the experimental results of the $3D$-dimensional switching field curve, the so-called Stoner-Wohlfarth astroid, it was assumed that a few outer layers in the truncated octahedral particle were magnetically "dead", leading to an effective elongation and thereby to a non-perfect octahedron. Producing such a faceted elongated particle by somehow cutting the latter is an arbitrary procedure. In order to minimize the changes in the surface structure caused by elongation, we assumed a spherical particle or introduced elliptical elongation along the easy axis. This kind of structure has been the basis of many theoretical studies using the Heisenberg Hamiltonian (see, e.g., Refs. 7,14,17,18,20,21,23).

Regarding the arrangement at the particle surface, an appropriate approach would be to use molecular-dynamic techniques[24,25] based on the empirical potentials for specific materials. This would produce more realistic non-perfect surface structures, more representative of what it is hinted at by experiments. However, these potentials exist only for some specific materials and do not fully include the complex character of the surface. Moreover, the particles thus obtained (see, e.g., Ref.26), may have non-symmetric structures, and may present some dislocations. All these phenomena lead to a different behavior of differently prepared particles which will be studied in a separate publication.

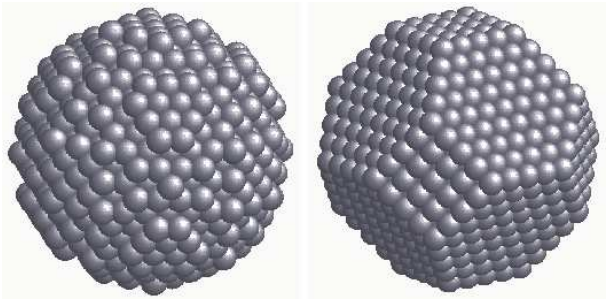

FIG. 1: Two particles cut from fcc structure: spherical (left) and truncated octahedron (right).

In the present work, in order to illustrate the general tendency of the magnetic behavior, we mostly present results for particles with "pure" non modified surfaces, namely spheres, ellipsoids and truncated octahedra cut from regular lattices. Even in this case, the surface arrangement may appear to be very different (see Fig. 1) leading to a rich magnetic behavior.

B. Spherical particles

We compute the $3D$ energy potential as a function of the spherical coordinates (θ, φ) of the net magnetization $\mathbf{m}$ of many-spin particle. We do this for a spherical particle with uniaxial anisotropy in the core and NSA, cut from an sc, fcc and hcp lattices, and for different values of the surface anisotropy constant, k_s. Fig. 2 shows energy landscapes for spherical particles cut from an sc lattice. One can see that as k_s increases the global minima move away from those defined by the core uniaxial anisotropy, i.e., at $\theta = 0, \pi$ and any ϕ, and become maxima, while new minima and saddle points develop which are reminiscent of cubic anisotropy. Now, in Fig. 3 we present the corresponding $2D$ energy potential ($\varphi = 0$). From this graph we see that the energy of the many-spin particle is well reproduceed by Eq. (14) when k_s is small, which shows that such many-spin particle can be treated as an EOSP with an energy that contains uniaxial and cubic anisotropies. However, as was shown in Ref. 21, when the surface anisotropy increases to even larger values this mapping of the many-spin particle onto an effective one-spin particle fails.

Repeating this fitting procedure for other values of k_s we obtain the plots of $k_{\rm ua}^{\rm eff}$ and $k_{\rm ca}^{\rm eff}$ in Fig. 4. We first see that these effective constants are quadratic in k_s, in accordance with Eqs. (9) and (11). In addition, the plot on the right shows an agreement between the constant

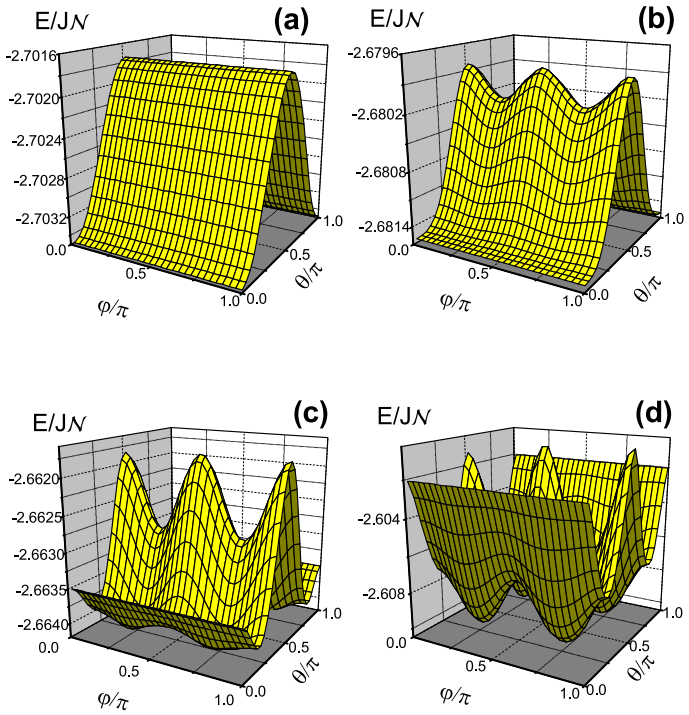

FIG. 2: Energy potentials of a spherical many-spin particle of $\mathcal{N} = 1736$ spins on an sc lattice with uniaxial anisotropy in the core ($k_c = 0.0025$) and NSA with constant (a) $k_s = 0.005$, (b) $k_s = 0.112$, (c) $k_s = 0.2$, (d) $k_s = 0.5$.

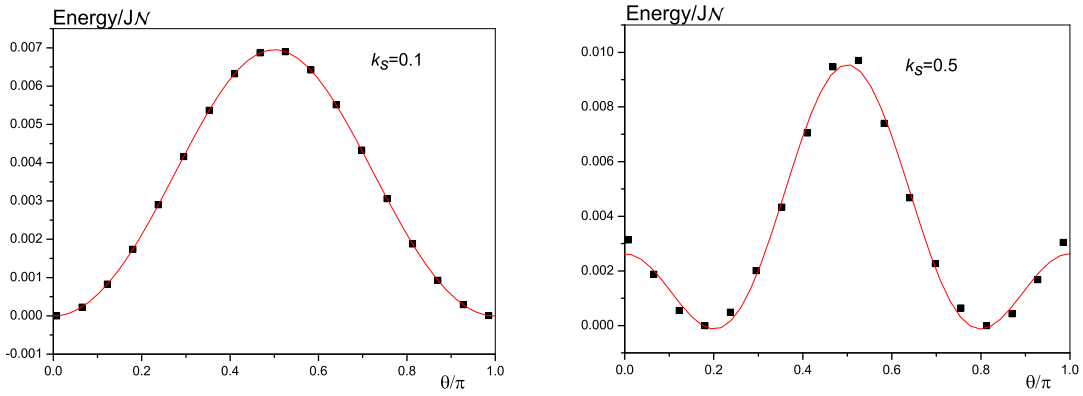

FIG. 3: (Shifted) $2d$ energy potentials of a spherical many-spin particle of $\mathcal{N} = 1736$ spins on an sc lattice with uniaxial anisotropy in the core ($k_c = 0.01$) and NSA with constant $k_s = 0.1$ (left), 0.5 (right). The solid lines are numerical fits to formula (14).

$k_{\rm ua}^{\rm eff} - \mathcal{E}_c$,, where $\mathcal{E}_c$ is defined by Eq. (7) in the uniaxial case. These results confirm those of Refs. 21,27,28 that the core anisotropy is modified by the surface anisotropy, though only slightly in the present case.

Comparing the energy potential in Fig. 2 for the sc and Fig. 5 for the fcc lattice one realizes that, because of the fact that different underlying structure produces different surface spin arrangements, the corresponding energy potentials exhibit different topologies. For instance, it can be seen that the point $\theta = \pi/2, \varphi = \pi/4$ is a saddle in particles cut from an sc lattice and a maximum in those cut from the fcc lattice.

Spherical particles cut from the sc lattice exhibit an effective four-fold anisotropy with $k_{\rm ca}^{\rm eff} < 0$ [see Fig. 4 and Eq. (14)]. As such, the contribution of the latter to the effective energy is positive, and this is compatible with the sign of $K_{\rm ca}$ in Eq. (9). In Figs. 6, 7 we plot the $2D$ energy potential and the effective anisotropy constants, respectively, for a spherical particle with fcc structure. For a spherical fcc particle, the effective cubic constant

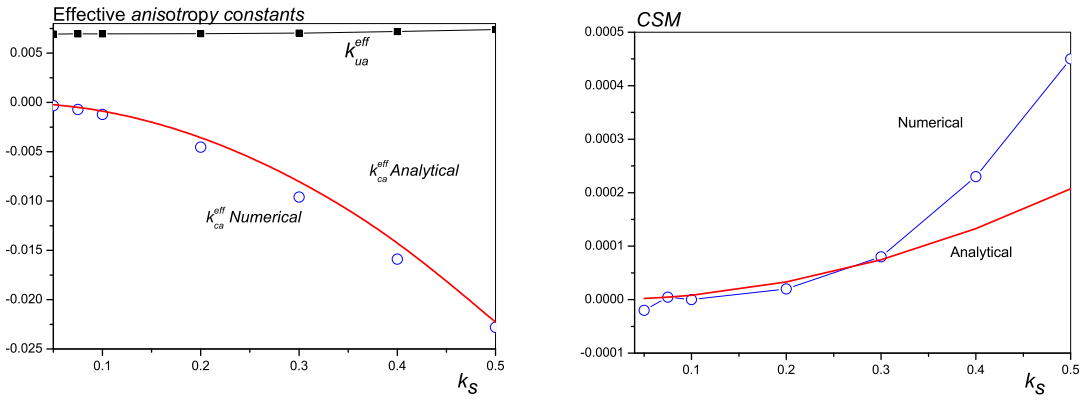

FIG. 4: Effective anisotropy constants against k_s for a spherical many-spin particle of $\mathcal{N} = 1736$ spins cut from an sc lattice. The panel on the right shows the CSM contribution obtained numerically as $k_{\rm ua}^{\rm eff} - \mathcal{E}_c$, where $\mathcal{E}_c$ is defined by Eq. (7) in the uniaxial case. The thick solid lines are plots of Eqs. (9) and (11) with $\varphi = 0$.

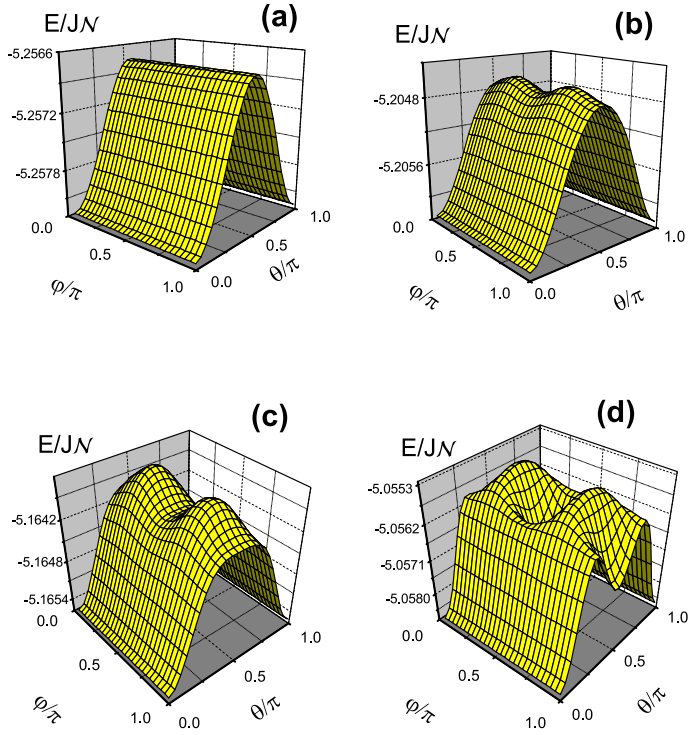

FIG. 5: Energy potentials of a spherical many-spin particle with uniaxial anisotropy in the core ($k_c = 0.0025$) and NSA with constant (a) $k_s = 0.005$, (b)$k_s = 0.1$, (c) $k_s = 0.175$, (d) $k_s = 0.375$. The particle contains $\mathcal{N} = 1264$ spins on an fcc lattice.

$k_{\rm ca}^{\rm eff}$ is positive [see Fig. 7], and as for the sc lattice, it is quadratic in k_s. As mentioned earlier, the coefficient κ in (9) depends on the lattice structure and for fcc it may become negative. To check this one first has to find an analytical expression for the spin density on the fcc lattice, in the same way the sc lattice density was obtained in Ref. 18 [see Eq. (6) therein]. The corresponding developments are somewhat cumbersome and are now in progress. Likewise, the coefficient $\tilde{\kappa}$ in Eq. (11) should change on the fcc lattice, thus changing the uniaxial and cubic contributions as well.

Finally, in particles with the hcp lattice and large surface anisotropy, we have found that the effective energy potential is six-fold, owing to the six-fold symmetry inherent to the hcp crystal structure. The global magnetization minimum is also shifted away from the core easy direction.

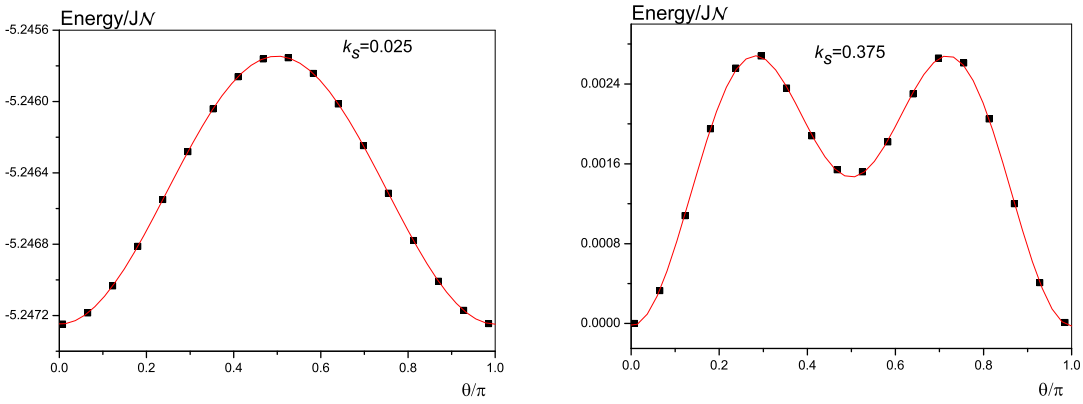

FIG. 6: The same as in Fig. 3 but here for the fcc lattice and $k_s = 0.025, 0.375$.

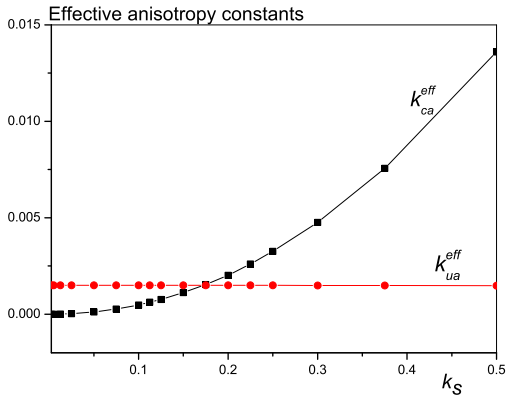

FIG. 7: Effective anisotropy constants against k_s for a spherical particle of $\mathcal{N} = 1264$ spins cut from an fcc lattice with uniaxial core anisotropy $k_c = 0.0025$. The lines are guides to the eye.

C. Ellipsoidal many-spin particles and effect of elongation

Now we investigate the effect of elongation. As discussed earlier, due to the contribution in Eq. (8), even a small elongation may have a strong effect on the energy barrier of the many-spin particle, and in particular on the effective uniaxial constant $k_{\rm ua}^{\rm eff}$, as will be seen below. Fig. 8 shows the energy potential of an ellipsoidal many-spin particle with aspect ratio 2:3, cut from an fcc lattice. Unlike the energy potentials of spherical particles, the result here shows that for large surface anisotropy the energy minimum corresponds to $\theta = \pi/2$. Indeed, due to a large number of local easy axes on the surface pointing perpendicular to the core easy axis, the total effect is to change this point from a saddle for small k_s to a minimum when k_s assumes large values. The effective uniaxial and cubic anisotropy constants are shown in Fig. 9. As expected the effective uniaxial constant shows a strong linear variation and even changes sign at some value of k_s, as opposed to the case of a spherical many-spin particle. On the other hand, as for the latter case, the constant $k_{\rm ca}^{\rm eff}$ retains its behavior as a quadratic function of k_s. Again, in the case of an sc lattice $k_{ca}^{\rm eff} < 0$ and on an fcc lattice $k_{ca}^{\rm eff} > 0$.

D. Truncated octahedral many-spin particles

Here we consider the so-called truncated octahedral particles. Real particles are often reported as having this structure with fcc underlying lattice [see, e.g. Co or Co/Ag particles in Ref. 1,2,4]. We perform the same calculations as before for a many-spin particle cut from an fcc lattice, with cubic single-site anisotropy in the core and NSA. In Fig. 10 we plot the dependence of the effective cubic constant $k_{\rm ca}^{\rm eff}$ as a function of k_s for $k_c > 0$ and $k_c < 0$. It can be seen that, similarly to the results discussed above, the effective cubic constant is again proportional to k_s^2 but now its increase with k_s is slower. This is mainly due to the two contributions, one coming from the initial core cubic anisotropy and the other from the surface contribution as in Eq. (9). The surface contribution can again change the sign of the initially negative cubic core anisotropy. Besides, we clearly see that the many-spin particle develops a negative uniaxial anisotropy contribution, induced by the surface in the presence of core anisotropy.

IV. ENERGY BARRIERS

A. Dependence of the energy barrier on k_s

Now we evaluate the energy barriers of many-spin particles by numerically computing the difference between

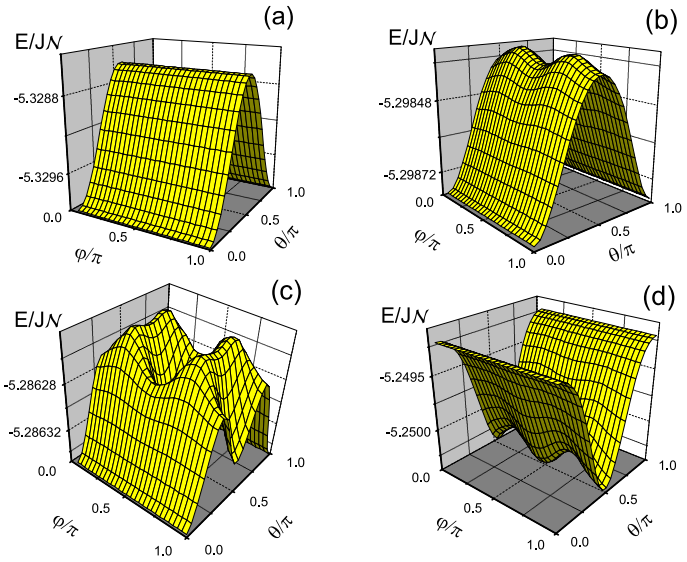

FIG. 8: Energy potentials of an ellipsoidal particle cut from an fcc lattice and with uniaxial anisotropy in the core ($k_c = 0.0025$) and NSA with constant (a) $k_s = 0.0125$, (b)$k_s = 0.075$, (c) $k_s = 0.1$, (d) $k_s = 0.175$.

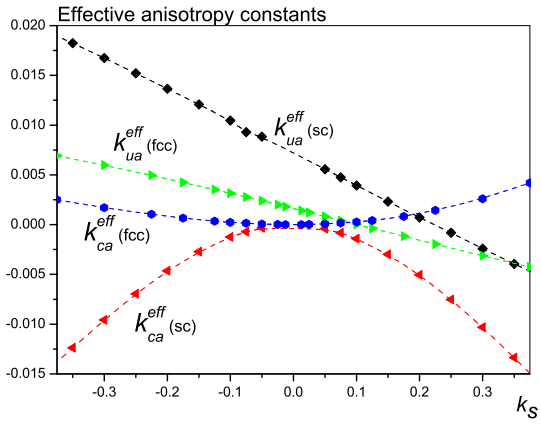

FIG. 9: Effective anisotropy constants against k_s for an ellipsoidal particle of $\mathcal{N} = 2044$ spins on sc and fcc lattices, with uniaxial core anisotropy $k_c = 0.0025$. The lines are guides.

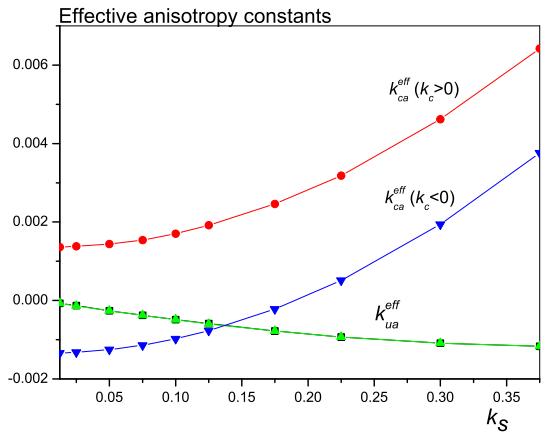

FIG. 10: Effective anisotropy constants against k_s for a truncated octahedral particle of $\mathcal{N} = 1080$ spins, fcc structure and cubic anisotropy in the core with $k_c > 0$ and $k_c < 0$.

the energy at the saddle point and at the minimum, using the Lagrangian multiplier technique described earlier. On the other hand, the EOSP energy potential (14) can be used to analytically evaluate such energy barriers and to compare them with their numerical counterparts. Namely, we have investigated minima, maxima and saddle points of the effective potential (14) for different values and signs of the parameters $k_{\rm ua}^{\rm eff}$ and $k_{\rm ca}^{\rm eff}$ and calculated analytically the energy barrier in each case. The results are presented in Table I. The energy barriers for the case $k_{\rm ua}^{\rm eff} > 0$ are plotted in Fig. 11. We remark that for large surface anisotropy $|\zeta| >> 1$, where $\zeta \equiv k_{ca}^{eff}/k_{ua}^{eff}$, all energy barriers are simple linear combinations of the two anisotropy constants.

Note that in a wide range of the parameters several energy barriers (corresponding to different paths of magnetization rotation) coexist in the system in accordance with the complex character of the effective potential with two competing anisotropies [see Figs. 2(c), 8(c)]. Because of this competition the symmetry of the anisotropy can be changed leading to relevant energy barriers in the θ or φ direction, the former case is illustrated in Fig.8(a,b,c), where switching occurs between global minima at $\theta = 0$ and $\theta = \pi$ and the latter is shown in Fig.8(d) where the large surface anisotropy has given rise to an easy plane with the stable states corresponding

TABLE I: Energy barriers for the effective one-spin particle. The critical angle $\theta_c(\phi)$ is defined by $\cos(\theta_c(\phi))^2 = (k_{\rm ua}^{\rm eff} + k_{\rm ua}^{\rm eff}(\sin(\phi)^4 + \cos(\phi)^4))/(k_{\rm ca}^{\rm eff}(1 + \sin(\phi)^4 + \cos(\phi)^4))$

$\zeta = k_{\rm ca}^{\rm eff}/k_{\rm ua}^{\rm eff}$	Minima(θ, φ)	Saddle points(θ, φ)	Energy barriers, $\Delta E_{\rm EOSP}$	
		$k_{\rm ua}^{\rm eff} > 0$		
$-\infty < \zeta < -1$	$\theta_c(\pi/4); \pi/4$	$\pi/2; \pi/4$	$k_{\rm ua}^{\rm eff}/3 - k_{\rm ca}^{\rm eff}/12 - (k_{\rm ua}^{\rm eff})^2/3k_{\rm ca}^{\rm eff}$	(1.1)
	$\theta_c(\pi/4); \pi/4$	$\theta_c(\pi/2); \pi/2$	$-k_{\rm ua}^{\rm eff}/6 - k_{\rm ca}^{\rm eff}/12 - (k_{\rm ua}^{\rm eff})^2/12k_{\rm ca}^{\rm eff}$	(1.2)
$-1 < \zeta < 0$	$0; 0$	$\pi/2; 0$	$k_{\rm ua}^{\rm eff} + k_{\rm ca}^{\rm eff}/4$	(2)
$0 < \zeta < 1$	$0; \pi/2$	$\pi/2; \pi/2$	$k_{\rm ua}^{\rm eff}$	(3)
$1 < \zeta < 2$	$\theta_c(0); \pi/2$	$\theta_c(\pi/2); \pi/2$	$k_{\rm ua}^{\rm eff}/2 + k_{\rm ca}^{\rm eff}/4 + (k_{\rm ua}^{\rm eff})^2/4k_{\rm ca}^{\rm eff}$	(4.1)
	$\pi/2; \pi/2$	$\theta_c(\pi/2); \pi/2$	$-k_{\rm ua}^{\rm eff}/2 + k_{\rm ca}^{\rm eff}/4 + (k_{\rm ua}^{\rm eff})^2/4k_{\rm ca}^{\rm eff}$	(4.2)
$2 < \zeta < \infty$	$0; \pi/2$	$\theta_c(\pi/2); \pi/2$	$k_{\rm ua}^{\rm eff}/2 + k_{\rm ca}^{\rm eff}/4 + (k_{\rm ua}^{\rm eff})^2/4k_{\rm ca}^{\rm eff}$	(5.1)
	$\pi/2; \pi/2$	$\pi/2; \pi/4$	$k_{\rm ca}^{\rm eff}/4$	(5.2)
	$\pi/2; \pi/2$	$\theta_c(\pi/2); \pi/2$	$-k_{\rm ua}^{\rm eff}/2 + k_{\rm ca}^{\rm eff}/4 + (k_{\rm ua}^{\rm eff})^2/4k_{\rm ca}^{\rm eff}$	(5.3)
		$k_{\rm ua}^{\rm eff} < 0$		
$-\infty < \zeta < -1$	$\pi/2; \pi/2$	$\theta_c(\pi/2); \pi/2$	$-k_{\rm ua}^{\rm eff}/2 + k_{\rm ca}^{\rm eff}/4 + (k_{\rm ua}^{\rm eff})^2/4k_{\rm ca}^{\rm eff}$	(6.1)
	$\pi/2; 0$	$\pi/2; \pi/4$	$k_{\rm ca}^{\rm eff}/4$	(6.2)
	$0; \pi/2$	$\theta_c(\pi/2); \pi/4$	$k_{\rm ua}^{\rm eff}/2 + k_{\rm ca}^{\rm eff}/4 + (k_{\rm ua}^{\rm eff})^2/4k_{\rm ca}^{\rm eff}$	(6.3)
$-1 < \zeta < 0$	$\pi/2; 0$	$\pi/2; \pi/4$	$k_{\rm ca}^{\rm eff}/4$	(7)
$0 < \zeta < 1$	$\pi/2; \pi/4$	$\pi/2; \pi/2$	$k_{\rm ca}^{\rm eff}/4$	(8)
$1 < \zeta < 2$	$\pi/2; \pi/4$	$\theta_c(\pi/2); \pi/2$	$-k_{\rm ua}^{\rm eff}/2 + (k_{\rm ua}^{\rm eff})^2/4k_{\rm ca}^{\rm eff}$	(9)
$2 < \zeta < \infty$	$\theta_c(\pi/4); \pi/4$	$\pi/2; \pi/4$	$-k_{\rm ua}^{\rm eff}/6 - k_{\rm ca}^{\rm eff}/12 - (k_{\rm ua}^{\rm eff})^2/3k_{\rm ca}^{\rm eff}$	(10.1)
	$\theta_c(\pi/4); \pi/4$	$\theta_c(\pi/2); \pi/2$	$k_{\rm ua}^{\rm eff}/3 - k_{\rm ca}^{\rm eff}/12 - (k_{\rm ua}^{\rm eff})^2/12k_{\rm ca}^{\rm eff}$	(10.2)

to $(\theta = \pi/2, \varphi = n * \pi/2)$ where n is an integer. In some cases there are multiple energy barriers, but here we consider only the relevant energy barrier for switching, corresponding to the lowest energy path between global minima.

We have seen that in the case of a spherical particle cut from an sc lattice, and in accordance with the EOSP energy potential (14), $k_{\rm ua}^{\rm eff} > 0$ and $k_{\rm ca}^{\rm eff} < 0$ [see Fig. 4]. For a spherical particle with an fcc lattice, $k_{\rm ua}^{\rm eff} > 0, k_{\rm ca}^{\rm eff} > 0$, as can be seen in Fig. 7. Finally, for ellipsoidal and truncated octahedral MSPs, the results in Figs. 9, 10 show that $k_{\rm ua}^{\rm eff}$ may become negative at some value of k_s, since then the contributions similar to (11) and (8) become important.

Fig. 12 shows the energy barrier of a spherical particle cut from an sc lattice as a function of k_s. The non-monotonic behavior of the energy barrier with k_s follows quantitatively that of the EOSP potential (14). Indeed, the solid line in this plot is the analytical results (2) and (1.1) from Table I, using analytical expressions of Eq. (9) together with the pure core anisotropy contribution (7). The discrepancy at the relatively large k_s is due to the fact that the analytical expressions are valid only if the condition (12) is fulfilled; the CSM contribution has not been taken into account.

Fig. 13 represents the energy barriers against k_s for particles with different shapes and internal structures. First of all, one can see a different dependence on k_s as compared to particles with the sc lattice. In the present

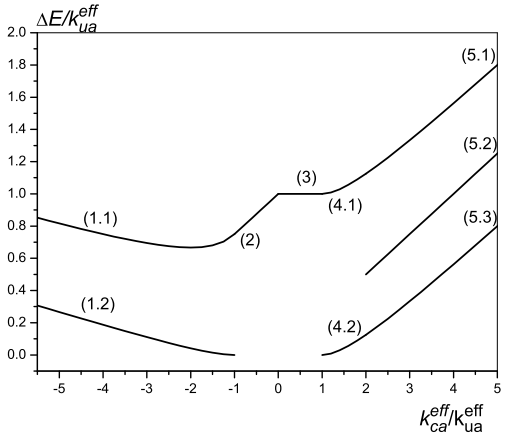

FIG. 11: Analytical energy barriers of the EOSP with the potential (14) as functions of $k_{\rm ca}^{\rm eff}/k_{\rm ua}^{\rm eff} = \zeta$ with $k_{\rm ua}^{\rm eff} > 0$. Analytical formulas from Table I are labelled.

case, i.e., $k_{\rm ua}^{\rm eff} > 0, k_{\rm ca}^{\rm eff} > 0$, the energy barriers are given by Eqs. (3) and (4.1) in Table I. Consequently, for small values of k_s with $|\zeta| < 1$ and neglecting the CSM term, the energy barrier is independent of k_s. Accordingly, the nearly constant value of the energy barrier, coinciding with that of the core, is observed for particles in a large

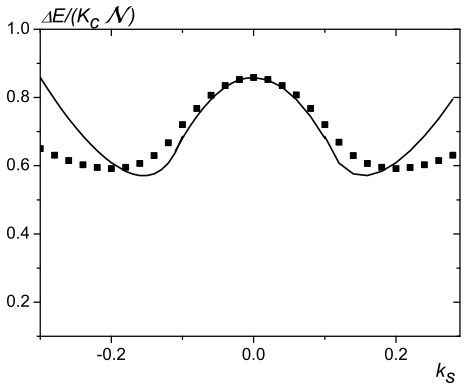

FIG. 12: Energy barrier as a function of k_s for a spherical particle cut from an sc lattice. The particle contains $\mathcal{N} = 20479$ spins and has the uniaxial core anisotropy $k_c = 0.0025$. The solid line is a plot of the analytical expressions (1.1) and (2) from Table 1, using Eqs. (7) and (9).

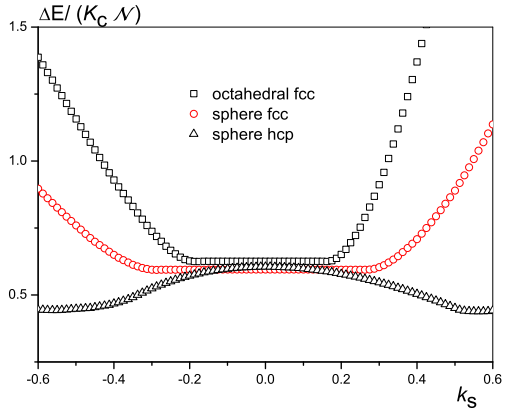

FIG. 13: Energy barriers against k_s for truncated octahedral particles cut from an fcc lattice ($\mathcal{N} = 1688$) and spherical particles cut from the fcc ($\mathcal{N} = 1289$) and hcp ($\mathcal{N} = 1261$) lattices. Uniaxial core anisotropy with $k_c = 0.0025$ is assumed.

range of k_s. For larger k_s, the energy barrier increases, since $k_{\rm ua}^{\rm eff} > 0$ for particles cut from an fcc lattice. At very large values of k_s, i.e., $k_s \gtrsim 100k_c$ the energy barriers strongly increase with k_s and may have values larger than that inferred from the pure core anisotropy.

The energy barriers for ellipsoidal particles are shown in Fig. 14. Note that in this case the effective uniaxial anisotropy constant $k_{\rm ua}^{\rm eff}$ is a linear function of k_s, according to the analytical result (8) and the numerical results presented in Fig. 9. Here, the energy barriers are not symmetric with respect to the change of sign of k_s. This is due to the fact that for $k_s < 0$ the effective uniaxial constant is a sum of the core anisotropy and the

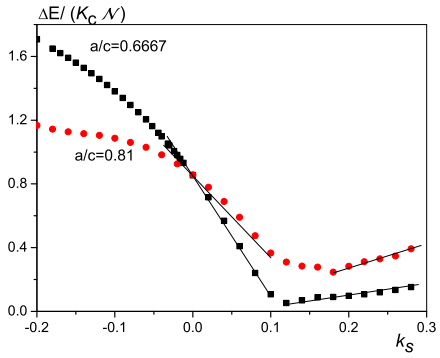

FIG. 14: Energy barriers versus k_s of ellipsoidal particles with different aspect ratio ($a/c = 0.6667, \mathcal{N} = 21121$, and $a/c = 0.81, \mathcal{N} = 21171$, with uniaxial core anisotropy $k_c = 0.0025$. The solid lines are linear fits.

first-order contribution owing to elongation. On the contrary, when $k_s > 0$, the "effective core anisotropy" $k_{\rm ua}^{\rm eff}$ is smaller than the pure core anisotropy $\mathcal{E}_c$ in Eq. (7). This means that at some k_s $k_{\rm ua}^{\rm eff}$ may change sign. At the same time the effective cubic anisotropy $k_{\rm ua}^{\rm eff}$ remains positive and is proportional to k_s^2. Accordingly, at the vicinity of the point at which $k_{\rm ua}^{\rm eff} \approx 0$ (see Fig. 9), rapid changes of the character of the energy landscape occur. The analysis, based on the EOSP potential shows that when $k_{\rm ua}^{\rm eff} > 0$ the energy barriers of ellipsoidal particles with sc lattice are defined by Eqs. (2) and (1.1) in Table I and for negative $k_{\rm ua}^{\rm eff} < 0$ these are given by Eq. (7) and (6.1) in Table I. Note that a regime of linear behavior in k_s exists for both $k_s < 0$ and $k_s > 0$ (see Fig. 14), specially when $k_s \lesssim 0.1(\zeta \ll 1)$. In some region of the effective anisotropy constants, e.g., $k_{\rm ua}^{\rm eff} > 0$, $|\zeta| < 1$, the energy barrier $\Delta E_{\rm EOSP} \approx k_{\rm ua}^{\rm eff}$, i.e., it is independent of the cubic contribution (neglecting again the CSM term). The interval of these parameters is especially large in fcc particles with $k_s < 0$, for which $k_{\rm ua}^{\rm eff}$ does not change sign and the energy barriers are exactly defined by Eq. (3) in Table I.

B. Dependence of the energy barrier on the system size

As $\mathcal{N} \to \infty$, the influence of the surface should become weaker and the energy barriers should recover the full value $K_c\mathcal{N}$. Fig. 15 shows energy barriers against the total number of spins $\mathcal{N}$ in particles of spherical shape cut from an sc lattice and with two values of $k_s > 0$. First of all, we note that in this case the main contribution to the effective anisotropy consists of two terms: the core anisotropy and the surface second-order contribution (9). In agreement with this all energy barriers of these particles are always smaller than $K_c\mathcal{N}$, since as we showed previously for the sc lattice, $k_{ca}^{\rm eff}$ is negative and

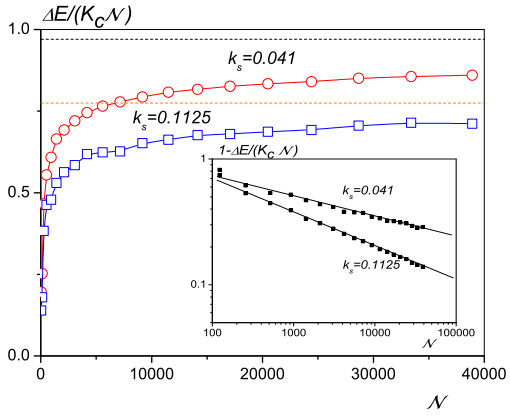

FIG. 15: Energy barrier as a function of the total number of spins $\mathcal{N}$ for two different values of the surface anisotropy, spherical particles cut from the sc lattice with uniaxial anisotropy $k_c = 0.0025$ in the core. The inset shows a slow dependence of the difference between these results and the uniaxial one-particle energy barrier $K_c\mathcal{N}$ in the logarithmic scale. The lines show analytical result Eqs.(7) and (9).

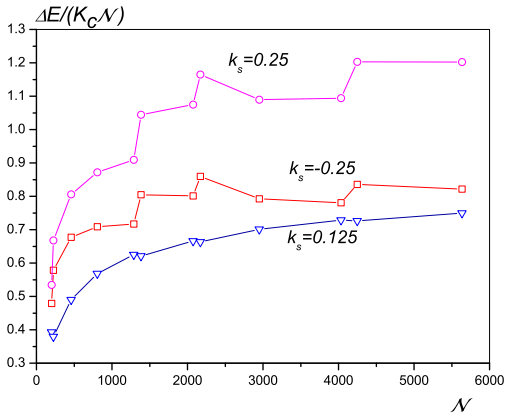

FIG. 16: Energy barriers versus $\mathcal{N}$ for truncated octahedra with internal fcc structure and uniaxial core anisotropy $k_c = 0.0025$.

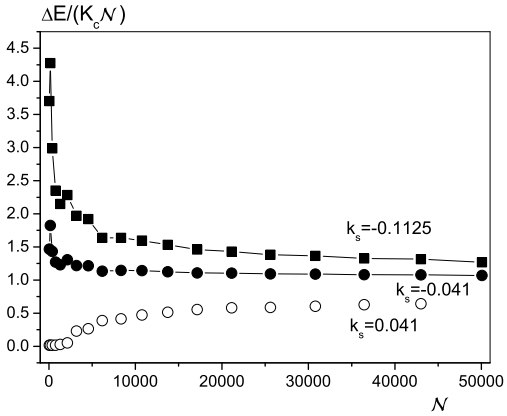

FIG. 17: Energy barriers as a function of the particle size for ellipsoidal particles with internal sc structure, uniaxial anisotropy $k_c = 0.0025$ and different values of k_s.

the energy barriers in this case are defined by Eq. (2) in Table I.

Both uniaxial core anisotropy (7) and the main contribution to the effective cubic anisotropy (9) scale with $\mathcal{N}$. As $\mathcal{N} \to \infty$, the core anisotropy contribution slowly recovers its full value, i.e., $\mathcal{E}_c/(K_c\mathcal{N}) \to 1$. However, from the analytical expressions Eqs. (7) and (9) even when $\mathcal{N} \to \infty$, when neglecting the CSM contribution, $\Delta E/(K_c\mathcal{N})$ should approach the value $1 - \kappa k_s^2/12k_c$, which is independent of the system size. Hence, we may conclude that it is the CSM contribution (11) that is responsible for the recovery of the full one-spin uniaxial potential. Being very small, this contribution produces a very slow increase of the energy barrier with the system size. In fact, we have estimated that even spherical particles of diameter $D = 20$ nm (an estimation based on the atomic distance of 4 Å) would have an effective anisotropy $\Delta E/(K_c\mathcal{N})$ that is 13% smaller than that of the bulk.

Truncated octahedra [see Fig. 16] show a behavior similar to that of the spherical particles. The energy barriers in this case behave very irregularly due to the rough variation of the number of atoms on the surface. The same effect was observed in other particles of small sizes. For truncated octahedra this effect arises as a consequence of non-monotonic variation of the number of spins on the surface for particles cut from regular lattices. The effective anisotropy of truncated octahedra particles with large $k_s > 0$ is larger than the core anisotropy in accordance with the fact that $k_{\rm ca}^{\rm eff}$ is positive for fcc structures and the energy barriers are defined by Eqs. (4.1) and (5.1) in Table I.

Finally, in Fig. 17 we present the energy barriers of ellipsoidal particles with different values of k_s and internal sc structure. The energy barriers in this case are defined by formulas (1.1) and (2) from Table I. The main contribution comes from the effective uniaxial anisotropy. The correction to it due to elongation is positive when $k_s < 0$ and negative in the opposite case. Consequently, particles with $k_s < 0$ have energy barriers larger than that inferred from the core anisotropy, and for those with $k_s > 0$ the energy barriers are smaller. In this case, the energy barrier approximately scales with the number of surface spins N_s (see Fig. 18), in agreement with the first-order contribution from elongation (11).

C. Applicability of the formula $\mathcal{K}_{\rm eff} = \mathcal{K}_\infty + 6\mathcal{K}_s/D$

The results presented above show that in the most general case, studied here, of a many-spin particle with NSA, this formula is not applicable, for the following reasons: (i) It assumes that the overall anisotropy of the particle remains uniaxial. However, we have shown that the surface anisotropy induces an additional cubic contribution. (ii) It assumes that the surface anisotropy always enhances that in the core. In the previous section we saw that both situations can arise. (iii) It is implicitly based on the hypothesis that the core and surface anisotropies are additive contributions. As we have seen above for large k_s (Table I) the energy barrier indeed can be represented as a sum of the effective cubic and uniaxial anisotropies. However, the cubic anisotropy term is proportional to k_s^2, which is inconsistent with formula (1). (iv) It assumes a linear dependence of energy barriers on the parameter $1/D$, or equivalently $N_s/\mathcal{N}$.

Consequently, spherical or octahedral particles cannot be described by formula (1), since in this case (i) No term linear in k_s is obtained. (ii) No term scales as the ratio of the surface-to-volume number of spins $N_s/\mathcal{N}$. However, in the case of elongated particles with a not too large surface anisotropy, (i.e., $|\zeta| < 1$ for fcc lattice or $|\zeta| << 1$ for sc lattice), the energy barriers are independent of the effective cubic anisotropy. In this case, for weakly ellipsoidal particles, for example, we may write

$$\Delta E_{EOSP} = k_{\rm ua}^{\rm eff} \approx k_c N_c/\mathcal{N} + A|k_s|/\mathcal{N}^{1/3} \qquad (16)$$

where A is a parameter that depends on the particle elongation and surface arrangement, and which is positive for $k_s < 0$ and negative in the opposite case. Hence, the behavior is as predicted by formula (1). An approximately linear behavior in $N_s/\mathcal{N}$ was also observed in the case of large surface anisotropy $\zeta >> 1$ (see Fig. 11). However, in the case at $\mathcal{N} \to \infty$, the "uniaxial anisotropy term" $\mathcal{K}_\infty$ is modified by the effective cubic anisotropy $k_{\rm ca}^{\rm eff} \sim k_s^2$. In Fig. 18 we plot the energy barriers of small ellipsoidal particles with sc structure, aspect ratio 2:3, and $k_s < 0$ from Fig. 17. For such particles, formula (1) should be modified as $\mathcal{K}_{\rm eff} = \mathcal{K}\infty + |\mathcal{K}_s|N_s/\mathcal{N}$. Accordingly, in Fig. 18 we plot the energy barrier against $N_s/\mathcal{N}$. These data are highly linear, especially when small particle sizes are removed, as shown by the fit in Fig.18. We note that in the case of relatively small surface anisotropy $k_s = -0.041$ (though 17 times larger than in the core), the full core anisotropy $\mathcal{K}_\infty = K_c/v$ (v is the atomic volume) can be extracted. However, for the larger surface anisotropy $k_s = -0.1125$, $\mathcal{K}_\infty$ is renormalized by the surface contribution (9). On the other hand, it not possible to extract the value of k_s, since the exact proportionality coefficient of Eq. (11) is dependent on the particles surface arrangement and elongation. The effective anisotropy constant $\mathcal{K}_s$ obtained from this fit is much smaller than the input value, namely, for $k_s/k_c = 45$ we obtain from the fit $(k_s/k_c)_{\rm eff} = 4.3$.

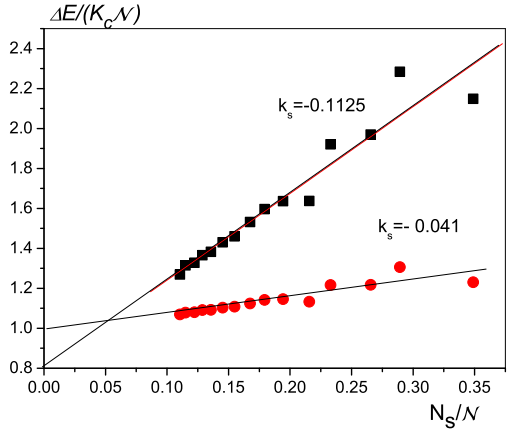

FIG. 18: Linear fit of energy barriers, versus the surface-to-total number of spins $N_S/\mathcal{N}$, of ellipsoidal particles with aspect ratio 2:3 with $k_s = -0.041$ (circles) and $k_s = -0.1125$ (squares).

V. CONCLUSIONS

We have studied in detail effective anisotropies and energy barriers of small magnetic particles within the Néel's surface anisotropy model. The calculations have been performed in a many-spin approach allowing deviations of the spins from the collinear state. They show that the magnetic behavior of small particles is rich and strongly dependent on the particle surface arrangement. The particular structure of each particle and the strength of its surface anisotropy makes each particle unique and its magnetic properties different in each case.

Our calculations show that the magnetic behavior of nanoparticles with Néel surface anisotropy and underlying cubic lattices is consistent with the effective model of one-spin particle with uniaxial and cubic anisotropies. The strength of this additional cubic anisotropy is dependent on many parameters, including the shape and elongation of the particles, and the underlying crystal structure which produces a different surface arrangement. The analytical results have made it possible to classify the various surface contributions and their effects as: (i) First order contribution from elongation (8), which produces an additional uniaxial anisotropy, is proportional to k_s and scales with the number of surface atoms. (ii) Surface second-order contribution (9) which is cubic in the net magnetization components, proportional to k_s^2 and scales with the particle's volume.(iii) Core-surface mixing contribution (11), which is smaller than the other two contributions and scales with both surface and volume of the particle.

In particles with sc lattices we compared analytical and numerical calculations for many-spin particles obtaining a very good agreement. Numerical modelling of particles with other structures has confirmed a general character

of these effects. The possibility to describe a variety of many-spin particles by a macroscopic magnetic moment with effective uniaxial and cubic anisotropies constant opens a unique possibility to model a collection of small particles in a multiscale manner, taking into account the surface effects through the effective potential (14).

Several very interesting effects were observed in particles with strong surface anisotropy. Particles with magneto-crystalline uniaxial anisotropy develop cubic anisotropy. At the same time the uniaxial anisotropy is also modified by the surface anisotropy. In ellipsoidal particles, surface anisotropy can change the sign of the effective uniaxial anisotropy. On the other hand, in particles with cubic magneto-crystalline core anisotropy, small uniaxial anisotropy appears. Some signatures of these behaviors may be found in the literature. For example in Ref. 1, the magnetic behavior of Co particles with fcc structure and, presumably, cubic magneto-crystalline anisotropy, have demonstrated the effect of uniaxial anisotropy.

The energy barriers of many-spin particles have been evaluated using the Lagrangian-multiplier technique. Their behavior could be well understood with the help of the effective one-spin particle potential (14). The energy barriers larger than $K_c\mathcal{N}$ have been obtained for all particles with very large surface anisotropy, $k_s \gtrsim 100k_c$, or for elongated particles with $k_s < 0$. This confirms a well-known fact that the surface anisotropy contributes to the enhancement of the thermal stability of the particle. However, in the case $k_s > 0$, the strength of the surface anisotropy has to be very strong.

We have found that the effective anisotropy value extrapolated from the energy barriers measurements is consistent with formula (1) only for elongated particles. In the case of relatively weak surface anisotropy k_s, the value of the core anisotropy could be correctly recovered. However, for larger k_s this effective uniaxial anisotropy $\mathcal{K}_\infty$ is renormalized by the surface. The applicability conditions of formula (1) are never fulfilled in spherical or truncated octahedral particles. The control of the parameters governing effective anisotropies does not seem to be possible in real experimental situations and therefore, the extraction of the parameters based on formula (1) in some cases may be unreliable.

On the other hand, we should note here that the conclusions of our work have been drawn on the basis of the Néel anisotropy model [see also Ref. 21 for the case of transverse surface anisotropy]. We would like to emphasize here that the model itself has a phenomenological character since it is not based on the spin-orbit coupling considerations. A more adequate approach should involve first principle calculations of the magnetic moments and MAE with atomic resolution, like in Co/Cu ([5,33]). However at the present state of the art this task remains difficult. Moreover, it is not clear how such models could be used to calculate, for example, thermal properties of small particles. The multiscale hierarchical approach[34] proposes to incorporate the ab-initio calculations into classical spin models. We conclude that more work on theory is necessary to understand surface magnetism, especially in relation with small particles.

Acknowledgments

This work was supported by a joint travel grant of the Royal Society (UK) and CSIC (Spain) and by the Integrated Action Project between France and Spain. The work of R.Yanes and O.Chubykalo-Fesenko has been also supported by the project NAN-2004-09125-C07-06 from the Spanish Ministry of Science and Education and by the project NANOMAGNET from Comunidad de Madrid. D. A. Garanin is a Cottrell Scholar of Research Corporation.

[1] M. Jamet, W. Wernsdorfer, C. Thirion, D. Mailly, V. Dupuis, P. Mélinon, and A. Pérez, Phys. Rev. Lett. **86**, 4676 (2001).
[2] M. Jamet, W. Wernsdorfer, C. Thirion, V. Dupuis, P. Mélinon, A. Pérez, and D. Mailly, Phys. Rev. B **69**, 24401 (2004).
[3] F. Bodker, S. Mörup, and S. Linderoth, Phys. Rev. Lett. **72**, 282 (1994).
[4] F. Luis, J. M. Torres, L. M. Garcia, J. Bartolome, J. Stankiewicz, F. Petroff, F. Fettar, J.-L. Maurrice, and A. Vaures, Phys. Rev. B **65**, 094409 (2002).
[5] Yu. Xie and J. Blackman, Phys. Rev. B **69**, 172407 (2002).
[6] C. Binns, S. H. Baker, K. W. Edmons, P. Pinetti, M. J. Maher, S. H. Louch, S. S. Dhesi, N. B. Brookes, J. Phys.: Condensed Matter **318**, 350 (2002).
[7] H. Kachkachi and M. Dimian, Phys. Rev. B **66**, 174419 (2002).
[8] L. Néel J.Phys Radium **15**, 376 (1954).
[9] R. H. Victora and J. M. MacLaren, Phys. Rev. B **47**, 11583 (1993).
[10] E. Tronc et al., J. Magn. Magn. Mater. **262**, 6 (2003).
[11] M. Respaud, J. M. Broto, H. Rakoto, A. R. Fert, L. Thomas, B. Barbara, M. Verelst, E. Snoeck. P. Lecante, A. Mosset, J. Osuna, T. Ould E. P. Lecante, A. Mosset, J. Osuna, T. Ould Ely, C. Amiens, and B. Chaudret, Phys. Rev. B **57**, 2925 (1998).
[12] D. A. Dimitrov and Wysin, Phys. Rev. B **50**, 3077 (1994).
[13] D. Weller, J. Stohr, R. Nakajima, A. Carl, M. G. Samant, C. Chappert, R. Megy, P. Beaucillain, P. Veillet, and G. A. Held, Phys Rev Lett; **75** , 3752 (1995).
[14] H. Kachkachi, A. Ezzir, M. Noguès, and E. Tronc, Eur. Phys. J. B **14**, 681 (2000).
[15] H. Kachkachi and D. A. Garanin, Physica A **300**, 487 (2001).
[16] H. Kachkachi and D. A. Garanin, Eur. Phys. J. B **22**, 291 (2001).

[17] O. Iglesias and A. Labarta, Phys. Rev. B **63**, 184416 (2001).
[18] D. A. Garanin and H. Kachkachi, Phys. Rev. Lett. **90**, 65504 (2003).
[19] H. Kachkachi and H. Mahboub, J. Magn. Magn. Mater. **278**, 334 (2004).
[20] H. Kachkachi and D. A. Garanin, in *Surface effects in magnetic nanoparticles*, edited by D. Fiorani (Springer, Berlin, 2005), p. 75.
[21] H. Kachkachi and E. Bonet, Phys. Rev. B **73**, 224402 (2006).
[22] E. Paz, F. Garcia Sanchez, and O. Chubykalo-Fesenko, unpublished (2006).
[23] R. H. Kodama and A. E. Berkovitz, Phys. Rev. B **59**, 6321 (1999).
[24] M. S. Daw and M. I. Baskes, Phys. Rev. Lett. **50**, 1285 (1983).
[25] F. Dorfbauer, T. Schrefl, M. Kirschner, G. Hrkac, D. Suess, O. Ertl, and J. Fidler, J. Appl. Phys. **99**, 08G706 (2006).
[26] R. Evans, U. Nowak, F. Dorfbauer, T. Schrefl, O. Mryasov, R. W. Chantrell, and G. Crochola, J. Appl. Phys. **99**, 086703 (2006).
[27] H. Kachkachi and D.A. Garanin, In preparation (2006).
[28] H. Kachkachi, *Effects of spin non-collinearities in magnetic nanoparticles* (Invited Paper at III Joint European Magnetic Symposia (JEMS), San Sebastian (Spain), 26-30 June 2006).
[29] R. Skomski and J. M. D. Coey, *Permanent Magnetism, Studies in Condensed Matter Physics Vol. 1* (IOP Publishing, London, 1999).
[30] K. B. Urquhart, B. Heinrich, J. F. Cochran, A. S. Arrott, and Myrtle, J. Appl. Phys. **64**, 5334 (1988).
[31] R. Perzynski and Yu. L. Raikher, in *Surface effects in magnetic nanoparticles*, edited by D. Fiorani (Springer, Berlin, 2005), p. 141.
[32] K. Yosida and M. Tachiki, Prog. Theor. Phys., **17**, 331 (1957).
[33] Y. Xie and J. Blackman, J. Phys.: Condensed Matter **16**, 3163 (2004).
[34] N. Mryasov, U. Nowak, K. Y. Guslienko, and R. W. Chantrell, Europhys. Lett. **69**, 805 (2005).